# Scanning Lagrangian Particle Tracking to measure 3D large scale aerodynamics of quadcopter flight

Daniel Schanz<sup>1,\*</sup>, Andreas Schröder<sup>1,2</sup>, Johannes Bosbach<sup>1</sup>, Tobias Strübing<sup>1</sup>, Claus C. Wolf<sup>1</sup>, Clemens Schwarz<sup>1</sup>, Alexander Heintz<sup>1</sup>

German Aerospace Center (DLR), Institute of Aerodynamics and Flow Technology, Göttingen, Germany
Institute of Transport Technology, Brandenburg University of Technology, Cottbus, Germany
\* Correspondent author: daniel.schanz@dlr.de

Keywords: Quadcopter aerodynamics, Lagrangian Particle Tracking, Shake-The-Box, Scanning, PTV

#### **ABSTRACT**

We present large-scale time-resolved and volumetric measurements of the flow surrounding a quadcopter drone. Cases with hovering flight, forward flight - with and without ground-effect - as well as lift-off scenarios have been realized. Five high-speed cameras were used to capture images of hundreds of thousands helium-filled soap bubbles being illuminated by pulsed LED arrays. The arrays were operated in a dual-scanning mode, where the front and the back part of the volume are illuminated intermittently, each with a frequency of 3 kHz. The cameras were recording at 6 kHz, thereby capturing both sub-time-series in a single measurement run. Compared to a full illumination of the volume, we can either reduce the number of particles imaged on the cameras given a fixed tracer concentration - facilitating the reconstruction - or operate at a higher tracer concentration while keeping the number of imaged particles fixed.

The dual time-series were evaluated by Lagrangian Particle Tracking, using the Shake-The-Box method, yielding dense fields of particle tracks. For the current results, the time series for both sub-volumes were evaluated independently. For the final contribution, an integrated evaluation scheme, alternatingly operating on both time-series is foreseen. After the tracking step, flow structures were identified using the data assimilation method FlowFit. The temporally and spatially highly resolved results document the strong interaction of the wakes induced by several rotors, as well as the interaction of wing tip vortices stemming from a single rotor. Brown-out effects are documented in forward flight. Averaged results of hovering flight enable an evaluation of the azimuthal distribution of the downwash- and outwash-velocities resulting from the geometric layout of the four rotors. By having highly resolved data encompassing the whole flight vehicle, the forces conveyed by the drone to the liquid can be determined via surface- or volume-integration.

### 1. Introduction

The wake of rotor aircraft is highly three-dimensional and unsteady. Quadcopter configurations as often used by current drones induce a downwash, whose center is characterized by a strong interaction of the individual wakes from the different rotors, while the outer zones are mostly

dominated by the interaction of subsequent blade tip vortices from the same rotor. The latter effect is also strongly present in helicopter wakes, with an additional strong interaction with the tail rotor wake. Due to the 3D character of these flows, certain features can only be revealed by volumetric measuring techniques. Wolf et al. (2019) applied Lagrangian particle tracking of Helium-filled soap bubbles (HFSBs,  $\sim 350~\mu m$  diameter; see Bosbach et al. 2009, Scarano et al. 2015) on parts of the wake of a model helicopter with a blade radius of R = 775 mm in a volume of approx. 0.1 m3. They found the first experimental evidences of S-shaped secondary vortex structures, connecting the main tip vortices. A comparable experiment was recently performed by Schröder et al. (2023) on a single blade rotor.

Lagrangian particle tracking (LPT) or Particle Tracking Velocimetry (PTV) are methods to characterize 3D flows by reconstructing the volumetric trajectories of suitable flow tracers. This is typically realized by recording time-resolved projections of the tracer particles on several spatially distributed cameras. For classical PTV the 3D reconstruction is performed by triangulation (Maas et al. 1992), which applies epipolar geometry of Lines-of-Sight (LOS) emanating from the particle image peaks in different cameras. Recently, iterative approaches to triangulation, like (advanced) Iterative Particle Reconstruction (IPR, Wieneke 2012, Jahn et al. 2021) have emerged. Tracking can be performed as a secondary process (Maas et al. 1992) or as an integrated procedure using a predictor/corrector scheme (Schanz et al. 2016). For an overview on recent LPT developments please see Schröder & Schanz (2023).

The most severe limitation to the 3D reconstruction process is imposed by the number of particles imaged on each camera and the volume depth where these particles are distributed. The larger the number of particle images per image area ( $N_I$ , measured in particles-per-pixel, ppp), the more ambiguities are present in the triangulation process, thereby creating false reconstructions ('ghost particles'). Likewise, the deeper the imaged volume, the more possibilities for randomly meeting LOS, which also increases the generation of ghost particles. Due to these reasons, the typical seeding density for triangulation-based methods was limited to around 0.005 ppp. Advanced IPR methods shift this limitation by around an order of magnitude, but still the number of trackable particles limits the resolvability of instantaneous flow structures.

To improve on this inherent limitation, the idea of illuminating only parts of the volume to restrict the perceived particle density was already pursued in 2005 by Hoyer et al. They set up a laser light sheet that was scanning the observation volume in ten planes using a rotating eight-faced prism. This way they were able to triple the reconstructed number of tracks from a low-Re turbulent flow to a number of 5,000, compared to a conventional PTV setup.

Recently, Kozul et al (2019) extended this approach, making use of the volumetric depth information to restrict the partner search within the triangulation procedure, thereby reducing the

occurrence of ghost particles. In a synthetic test case they reconstructed 12 subvolumes using standard triangulation schemes, each with a particle image density of approx.  $N_I = 0.01$  ppp. The combination of the 12 subvolumes leads to an effective particle image density of around 0.125 ppp. The Shake-The-Box algorithm (STB, Schanz et al. 2016) is able to reach such  $N_I$  even without scanning due to the use of IPR and the predictor/corrector scheme. In this work we want to give first experimental evidence that the working range of STB can be further extended using a scanning approach. Here we used only a two-staged scanning, but the scheme is easily extendable to more sub-volumes (planes).

Furthermore, the experiment gives unprecedented experimental insight into the large-scale wake and inflow of a quadcopter drone in flight.

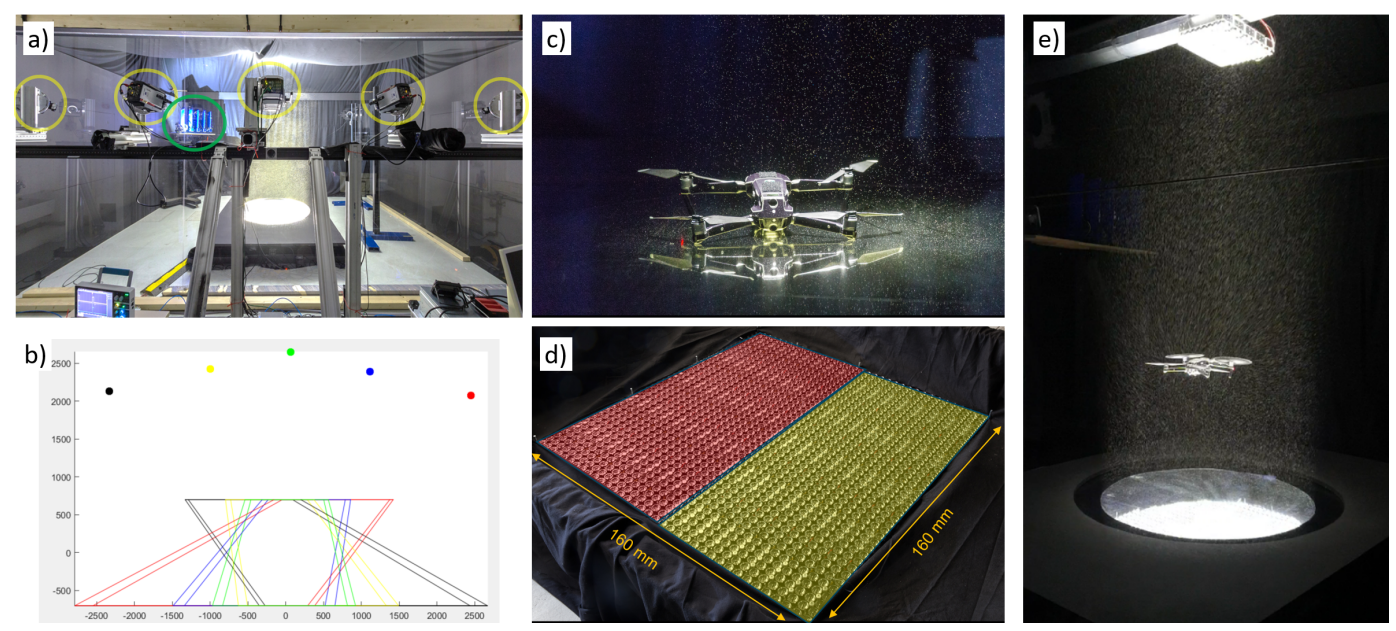


Figure 1 Experimental setup. (a) 72 m3 test room with floor LED array (blue), HFSB seeding rake (green) and five cameras (yellow) installed behind a polycarbonate glass wall; (b) top view of calibrated camera system, indicating common illuminated volume of ~ 1.85 m3; (c) photograph of the DJI Mavic 2 pro quadcopter; (d) the floor LED array without circular mask. Front Array marked in red, back array in yellow; (e) the drone in hovering flight, illuminated by floor and ceiling LEDs and surrounded by HFSB bubbles.

# 2. Experimental set-up and procedure

Building upon the work in Wolf et al. (2019), we present a time-resolved experimental investigation of quadcopter wakes, in volumes of up to  $1,85 \text{ m}^3$ , thus comprising the full volume around the used models, being a DJI Mavic 2 pro quadcopter drone (56 cm diameter with a blade radius of 11 cm, see Figure 1c) and a model helicopter with 45 cm blade length (not shown in this abstract). To this end, a large test room of  $6\times4\times3.4=82 \text{ m}^3$  was prepared with blackened walls on three sides and a tent-like ceiling ( $\sim4m$  crest height), constructed from black cloth (see Figure 1a). In this room, a quadcopter

drone was operated in several flight conditions (hovering, take-off/landing and forward flight, each with and without ground effect). The room was filled with HFSBs of approx.  $450 \,\mu$ m diameter prior to a recording, which were illuminated by a large array of LEDs on the floor ( $1.6 \times 1.6 \,\text{m}^2$  with a round aperture of  $1.25 \,\text{m}$  diameter) and a smaller one on the ceiling to illuminate the region shadowed by the flight object (Figure 1 d and e).

The cameras system consisted of four Vision Research Phantom v2640 and one v1840 cameras, operated at 6 kHz and recording 16,870 consecutive images per run. The three central cameras were equipped with 50 mm Zeiss Planar lenses, while the two outer cameras used f = 60 mm Zeiss Makro-Planar lenses. To realize a rudimentary two-plane scanning, the triggering of the LEDs was separated in a way that the front and back part of the array (in regard to the camera) were each triggered at 3kHz, with a delay of 1/6000 s between the two sub-arrays. Figure 2 shows two consecutive images captured with one of the measurement cameras from a case with the drone in hovering flight with ground effect. Seeding densities of more than 0.1 ppp per subvolume were realized (see detail view in Figure 2). This way the camera system was able to capture both time-series for 8435 consecutive images at 3kHz within the time-series of 16,870 images recorded at 6 kHz.

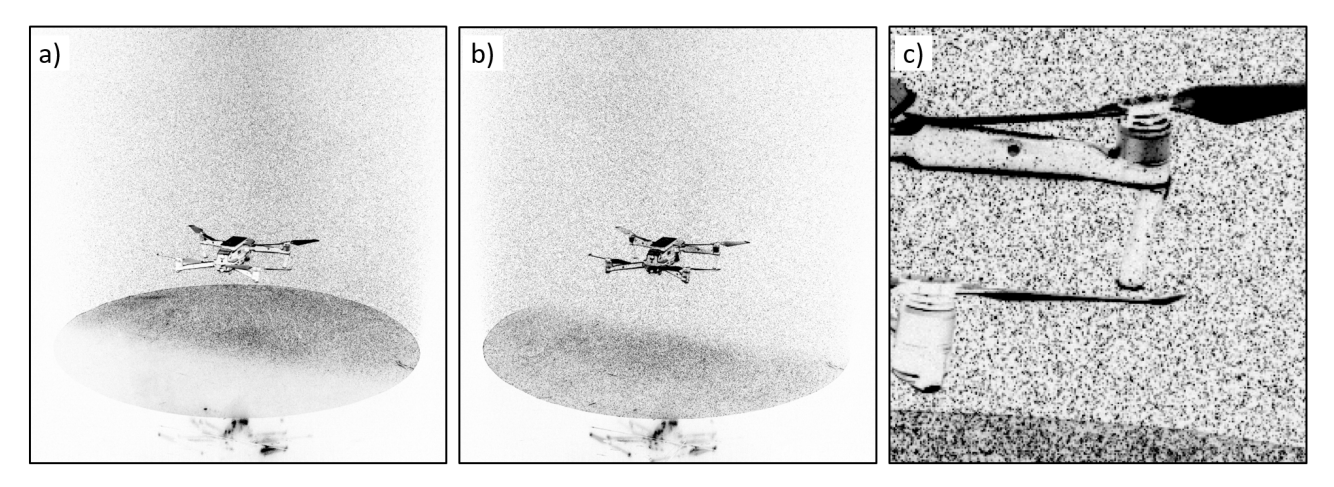


Figure 2 Exemplary b/w-inverted images from selected camera. a) 'back' part illuminated by triggering the far half of the LED array in relation to the camera system; b) 'front' part illuminated by triggering the close half of the LED array in relation to the camera system (recorded with a phase shift relative to a) of  $\Delta_t/2 = 1/6000$  s); c) detail view from a).

## 3. Results and discussion

The camera system was calibrated by placing a large calibration target ( $2.5 \times 1.25 \text{ m}^2$ ) in the center of the illuminated volume and traversing it  $\pm$  500 mm within the main viewing direction of the

cameras (here always the y-coordinate). From the recordings of the target at different volume depths, a two-plane calibration model (Wei and Ma 1991) was calibrated for each of the cameras. The geometrical calibration was further refined using Volume-Self-Calibration (VSC, Wieneke 2008) and a 2D-field correction of the residual calibration errors that cannot be described by the second order camera model (Schanz et al. 2019). The particle imaging properties are characterized by a calibration of the Optical Transfer Function (OTF, Schanz et al. 2013).

Preprocessing of the images was optimized to remove as much intensity of the imaged quadcopter as possible, while still retaining peaks visible in front of it. The first step is to subtract the minimum image of each run. Secondly, a mask is created based on the intensity of a Gaussian smoothing of the image. Within the mask, the intensity of the Gaussian smoothed image is subtracted from the original image. This procedure restricts the region of influence of the filter to connected bright regions (only the reflecting parts of the drone), while retaining the peaks visible on top of the bright areas by subtracting a local average intensity. Figure 3 demonstrates the effects of image preprocessing for a single camera.

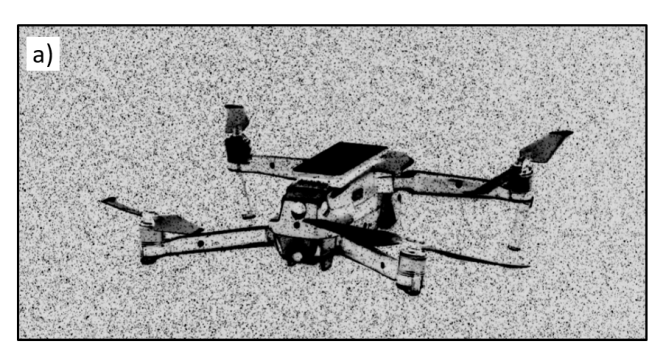




**Figure 3** Image preprocessing for removal of background and the bright regions of the imaged quadcopter: a) original camera image b) preprocessed image

The preprocessed images were evaluated using the DLR implementation of the Shake-The-Box (STB) method (Schanz et al. 2016). In the current state, the two time-series from front and back illumination were reconstructed independently. For each of the time-series, a separate tracking was performed using an advanced Variable-Timestep STB processing (Schanz et al. 2021): the cameras capture both fast particles in the wake of the rotors, as well as large quantities of slowly moving particles in the bulk surrounding the drone. The slow movement of these particles relative to the recording frequency can be detrimental to the tracking performance; this effect can be avoided by using different evaluation frequencies for the particles from different velocity regimes (for details see Schanz et al. 2021). The evaluation consists of four passes with three different time-separations. The first pass uses a time-separation of  $\Delta_S = 15$  time-steps and tracks the particles in the bulk. The second pass, going backward in time uses  $\Delta_S = 8$  time-steps and adds some faster

particles to the tracking system. The third pass, going again forward in time, uses  $\Delta_S=1$  time-step (therefore using all available images) and adds the missing fast particles. In the end a fourth pass with  $\Delta_S=1$  - but walking backwards in time - is performed to retrace all tracked particles to their first appearance in the measurement domain.

Evaluations of the case with the drone in hovering flight close to the ground shown in Figure 2 yield approx.

354,000 instantaneously tracked particles for the 'back' time-series and approx. 338,000 for the 'front' time-series. As can be seen from Figure 2, the full resolution of 4 MPix cannot be used in this case, instead an image area of approx. 2.8 MPix is filled with particle images. Each of the time-series is therefore operating at an effective particle image density of around 0.125 ppp.

Figure 4 a) and b) show the velocity vectors for the two time-series of a singular time-step. It can be seen that due to the use of LEDs that emit light with an opening angle of around 7°, the two sub-volumes are overlapping to a certain extent and the particles in the middle of the volume are reconstructed in both time-series. The perceived, or effective, seeding density from the combined sub-volumes is estimated to be around 0.2 ppp. The use of LEDs with a narrower opening angle or of a scanning laser light sheet would allow for less overlap, thereby increasing the effective seeding density and with it the value of particles per volume (ppv). On the other hand, in this experiment the overlap region coincides with the most interesting region of the quadcopter wake, where strong accelerations due to the interaction of the tor wakes occur. By modifying the processing to operate in a way that integrates the two time-series in a single evaluation, the particles in the overlap region can be tracked a temporal resolution of 6 kHz for an enhanced capturing of high-acceleration events. To this end, the STB scheme will have to be modified in a way that it can cope with the fact that the majority particles is only visible in every second image. Currently, tracks will be terminated if the intensity of the tracked particle falls below a certain threshold. The algorithm has to be informed about which particles are visible at what time. To this end, the volumetric light intensity of each sub-volume will be determined and used as a weighting factor. Based on this factor, the algorithm can decide whether a particle is visible for the current time-step or not. If it is not regarded as visible, it's (predicted) position will not be altered by shaking, nor will it be deleted due to the intensity threshold. As a result of these modifications, the Lagrangian tracks of the HFSB will extend over both sub-volumes at double the recording frequency of each time-series (here 6 kHz). Once the procedure has been implemented it can be easily adapted to cope with more than two scanned (sub-)volumes.

Figure 4 c) visually combines the two individual time-series by showing velocity vectors from both reconstructions for three consecutive time-steps. For better clarity, only particles with a velocity magnitude larger than 3m/s are shown. The wake of the four rotors is evident. The fast flow is

impacting onto the ground plate and the flow is diverted and spreading circularly from the central point. Vortical structures can be identified in the particle field.

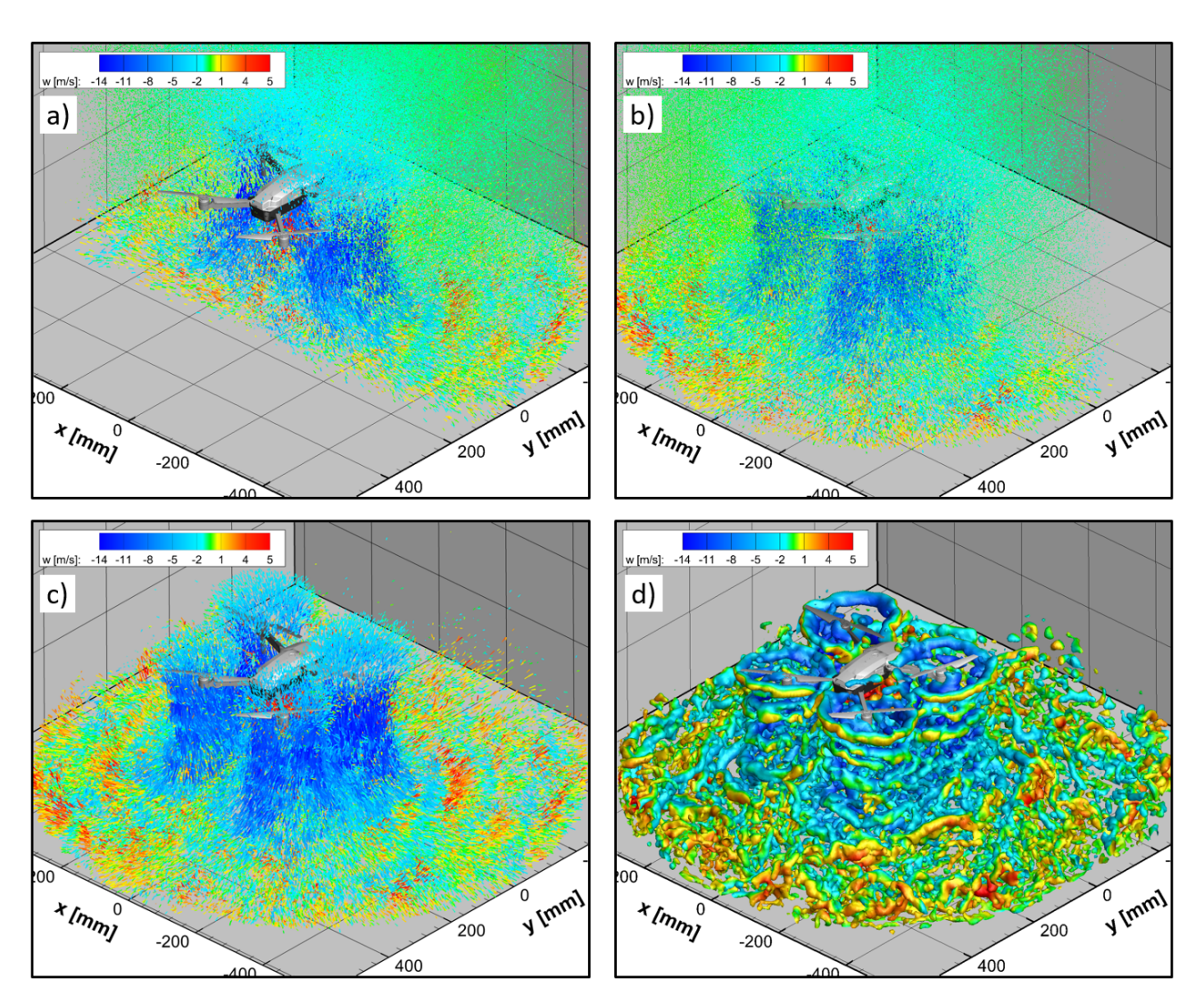


Figure 4 Experimental results of the scanning LPT experiment for hovering flight with ground effect. a) Velocity vectors of a single time-step for the 'back' part of the volume; b) the same for the 'front' part; c) combination of the two parts for the same time-step. Particles with a velocity lower than 3 m/s are blanked; d) FlowFit data assimilation result of the same time step, showing isosurfaces of Q-criterion ( $Q = 20,000/s^2$ ). Please note that the phase of the rotors of the rendered Quadcopter is not synchronized to the measurement.

For better understanding of the instantaneous flow field, the discrete values of velocity and acceleration at the particle locations are interpolated to a Cartesian grid in a Eulerian frame of reference. To this end, the data assimilation method FlowFit3 (Gesemann et al. 2016, Godbersen et al. 2024) is applied, which reconstructs continuous functions of velocity, velocity gradients and pressure of single time-steps. It applies physical constraints given by the governing equations to

increase the spatial resolution beyond the sampling by the particles. Figure 4 d) shows the result of applying FlowFit to the particles from Figure 4 a-c). The individual wakes of the four rotors emerge as spirals of vortices, being transported downwards towards the wall, where they are decomposed into less coherent structures. Beneath the center of the quadcopter, a region with upward flow is visible, documenting a so-called fountaining effect.

For these initial results, the temporal shift between the two sub-volumes was simply ignored. In the overlap region the particles from both sub-volumes were jointly used, resulting in a double representation of the particle tracks in this region. No apparent effects of these measures are visible within the instantaneous FlowFit results. However, the planned integrated evaluation (see previous paragraph), will ensure that each particle is represented only once at a harmonized timing.

Figure 5 displays results from an experimental realization of forward flight in ground effect (height of the quadcopter: 0.55m - approx. one drone diameter). Three different points in time, separated by 166.6 ms, are provided for a better understanding of the temporal dynamics. When entering the measurement domain, the quadcopter is pushing a strong frontal bow wave of small structures, while the main wake of the rotors is inclined in flight direction. The bow wake shows an asymmetry, which might be caused by history effects. Effects of brown-out (situations where the vision of a pilot is blocked by dust or dirt that is stirred up by the wake of an aircraft) are visible (see middle row), where vortical structures of the bow wave are piling up and are eventually drawn into the rotors. The rear wake of the quadcopter remains comparatively flat and attached to the wall.

Figure 6 shows several views on a single time-step from the same time-series of a forward flight maneuver in ground effect. The particle data from this time-step (Figure 6 a) were interpolated using the non-linear version of FlowFit3 (Godbersen et al. 2024), giving access to the pressure field (Figure 6 b). The wakes of all four rotors are visible as extended regions of negative pressure, retracing the main vortices. The low-pressure regions approach the ground both to the sides, as well as in the front of the quadcopter, where an extended region of negative pressure is formed around the rotating bow wave that is pushed forward by the approaching vehicle. In the stagnation region below the drone, a distinct region of positive pressure is created, which extends approx. one drone diameter behind the drone. The regions of positive pressure atop the rotors are likely artifacts of the pressure jump in the rotor plane. The particle tracking cannot follow the strong acceleration (and the bubbles are mostly hidden by the rotors themselves), so that the tracking system does not describe the impulse entry. To fulfill the momentum equation FlowFit creates a region of positive pressure to account for the undescribed impulse jump.

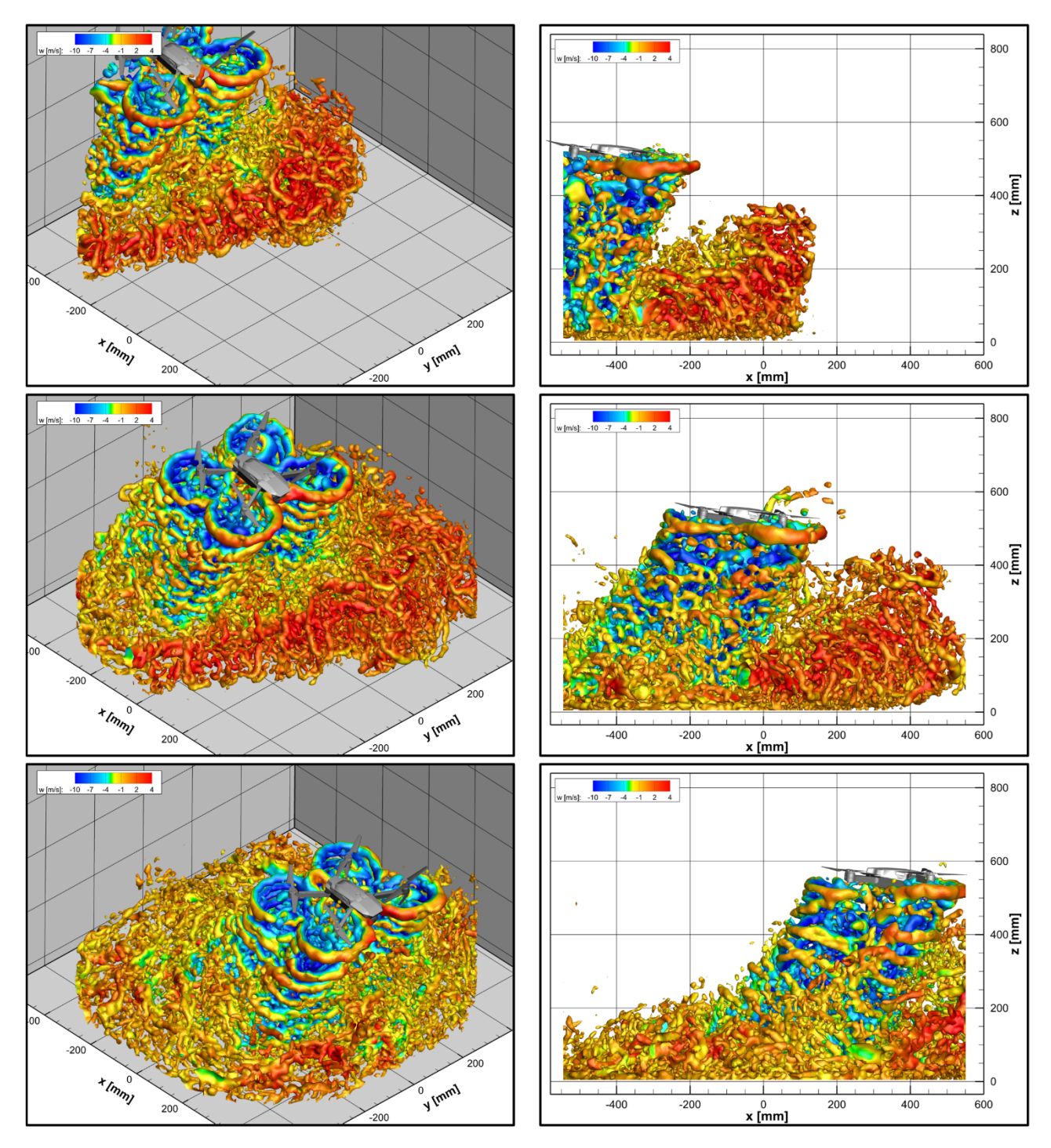
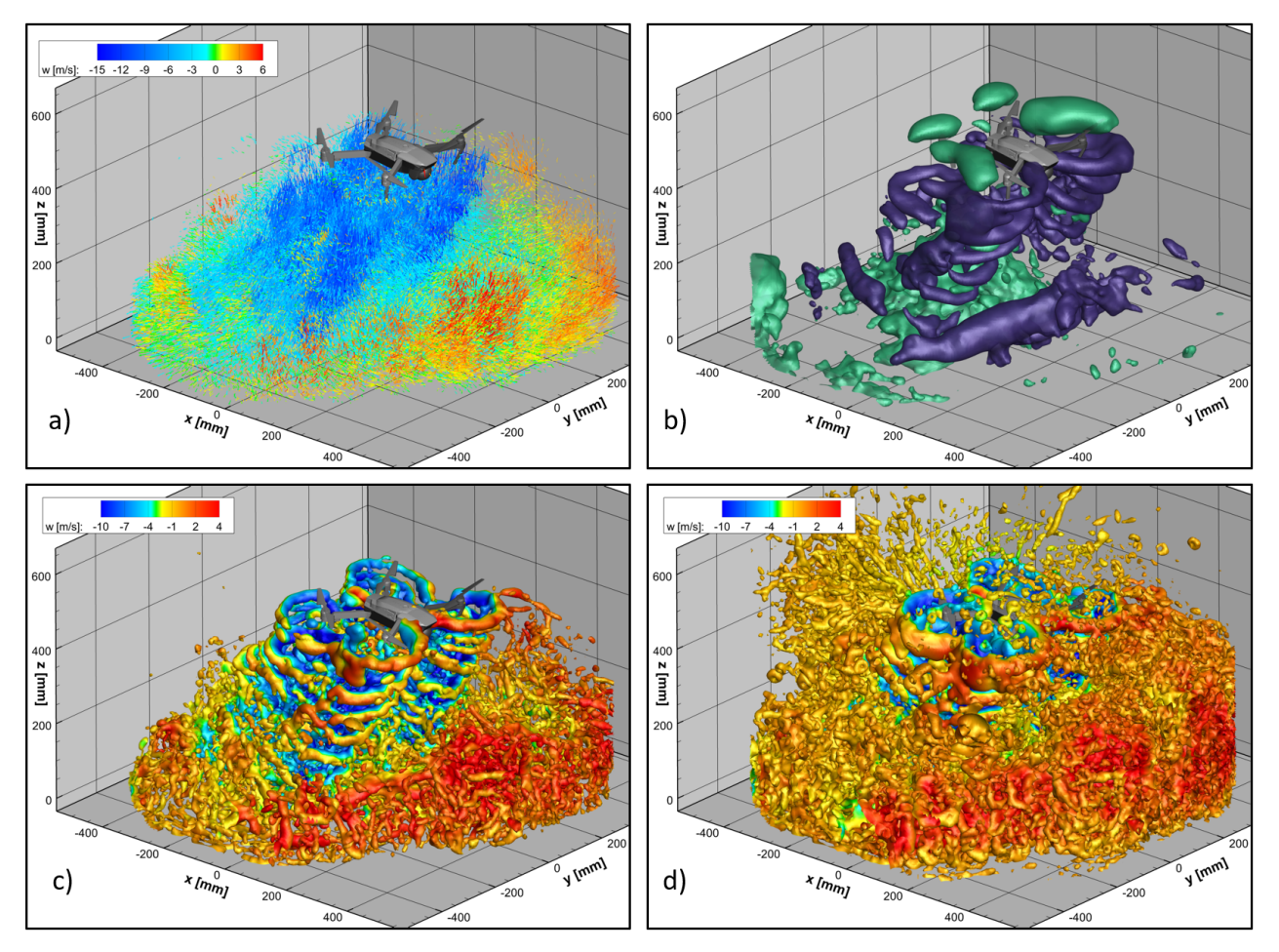


Figure 5 Isosurfaces of Q-criterion ( $Q=5,000 / s^2$ ) of a forward flight maneuver in ground effect at three subsequent times from two perspectives (left and right column). Time separation between frames: 500 time-steps (166.6 ms). Results gained by FlowFit interpolation of tracks from scanning STB-evaluation ( $\sim$ 300,000 tracked particles per sub-

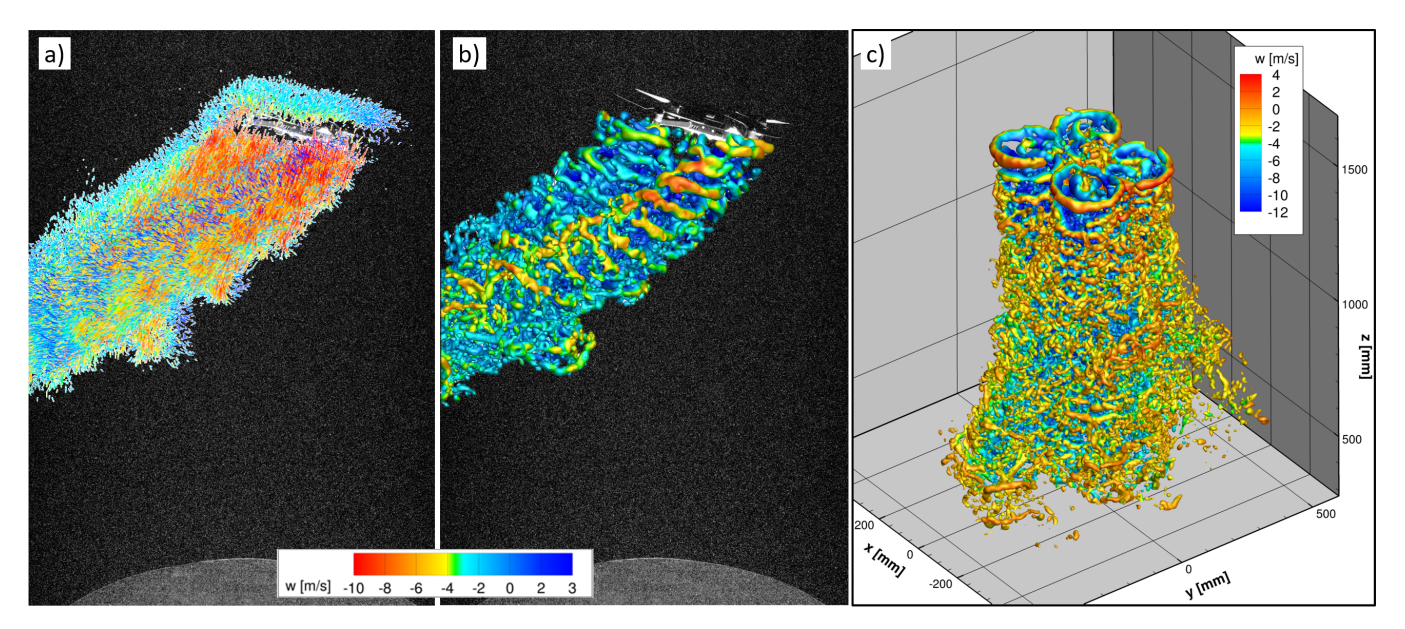
volume). The drone is rendered for visualization purposes only. Neither position nor phase were adapted to the data.

Figure 6 c) and d) compare the vortex system of the same flow situation at two different isosurface values of Q-criterion. While for a threshold of  $Q=10,000/s^2$ , the vortex system seems to be restricted to the main vortices of the rotors and their interaction with the ground, the lower threshold ( $Q=500/s^2$ ) reveals a whole system of previously unnoticed vortices. The temporal evolution (not visualized here) shows that these are mainly following the quadcopter wake and are being stretched by the departing pressure minimum. Above the drone singular weak vortices are detected, which are eventually drawn into the wake as well, after the drone has passed beneath them.



**Figure 6** Instantaneous snapshot from forward flight maneuver in ground effect. a) Velocity vectors, while blanking particles with a velocity lower than 2.5 m/s; b) isosurfaces of positive and negative pressure purple: -12 m<sup>2</sup>/s<sup>2</sup>; cyan:  $5 \text{ m}^2/\text{s}^2$ ); c) Isosurfaces of Q-criterion (Q=10,000/s<sup>2</sup>); d) Isosurfaces of Q-criterion (Q=500/s<sup>2</sup>)

Examples for test cases with the quadcopter located further away from the ground are provided in Figure 7 for hovering and forward flight. In these cases, a much longer development of the rotor wakes can be observed. While the wake structures are quickly interacting in the central parts beneath the quadcopter, long-lived structures can be identified in the outer regions, especially for the forward flight case, where coherent structures created by the rotors can still be seen more than one quadcopter diameter away from the drone. In the hovering case these structures seem to be decomposed more quickly into secondary structures, likely due to the more stationary turbulent field.



**Figure 7** Snapshots from evaluations of forward and hovering flight out of ground effect. a) Forward flight: Particles tracked by STB (blanked for velocity magnitude < 3 m/s), overlaid on camera image; b) Isosurfaces of Q-criterion (Q =  $15,000/\text{s}^2$ ) from FlowFit processing of the same time-step; c) Hovering flight: Isosurfaces of Q =  $10,000/\text{s}^2$ 

Figure 8 shows the time-averaged downwash velocity component w, calculated for a quasistationary hover test case and a time interval of about 2.33 s (7,000 flow samples). Shortly below the quadcopter, Figure 8 a), the four rotor wakes appear as individual and separated circular structures. The velocity distributions indicate a higher trust of the front rotors, which is probably a result of the quadcopter's weight distribution. Ongoing evaluations will show if transient rotor speed variations commanded by the position regulation also play an additional role. Moving in downstream direction by 0.5 m, Figure 8 b), the four wakes subsequently merge into a single, radially almost symmetric structure. In Figure 8 c), about 1 m below the quadcopter, a "plus"-shaped pattern of high downwash velocities emerges between the rotors, as indicated by black arrow markers. Figure 8 d) gives an impression of the streamwise evolution of this pattern by means of the volumetric isosurfaces for w = -8 m/s. It is noted that the azimuthal velocity

characteristics of VTOL aircraft with distributed propulsion is highly relevant for the operational safety, for example, see (CAA 2023).

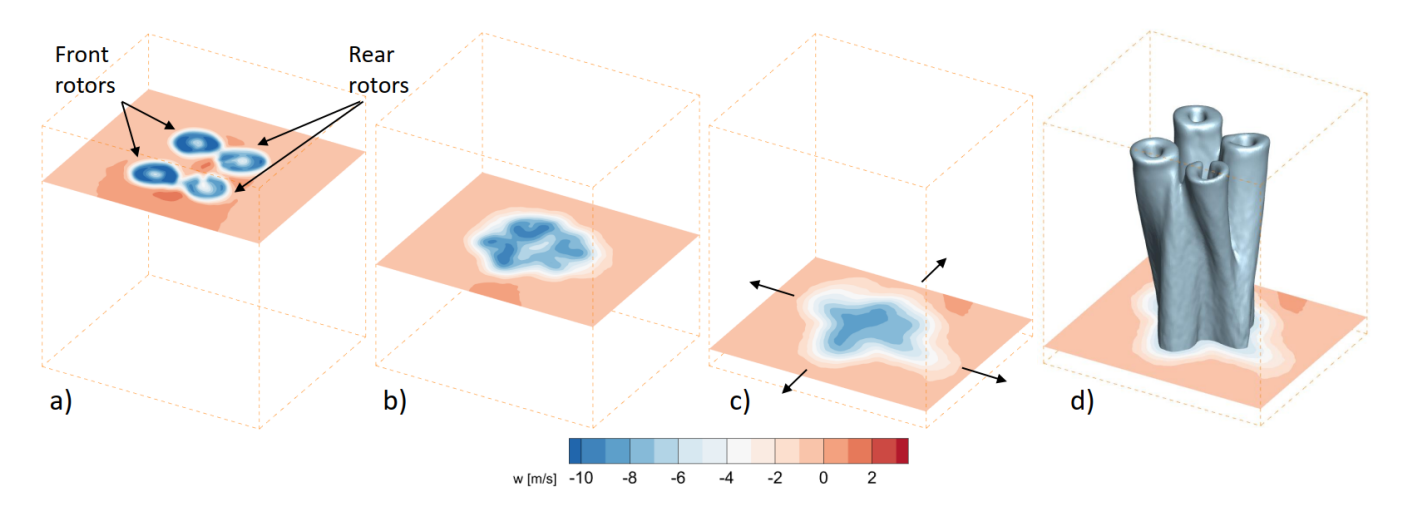


Figure 8 Evolution of the time-averaged downwash velocity over  $\Delta t = 2.33$  s in hover conditions. a), b), c): Horizontal slice planes with a vertical offset of  $\Delta z = -500$  mm. d): Same as c), but additionally showing volumetric isosurfaces for a downwash velocity of 8 m/s.

The availability of well-resolved velocity data all around the drone can be used to calculate the force generated by the four rotors of the quadcopter. This was done for a hovering case out of ground effect by defining a cubical reference volume around the drone and determining the surface integral of the momentum flux via the continuous velocity information from FlowFit reconstructions. The result is a temporally resolved value for the total force exerted by the drone to keep it hovering and is given in Figure 9. The observed fluctuations are likely due to the manual and automatic maneuvers to keep the drone as steady as possible. Also, due to the different velocities above and below the drone, the effect of a steering or balancing effort will travel faster to the lower control surface, leading to a momentary imbalance of the gained total momentum flux. These effects could by mitigated by using results from the extended non-linear version of FlowFit3 (Godbersen et al. 2024), which gives access to the continuous fields of velocity, acceleration, pressure and viscous stresses. With this information, a full volume integration of the forces according to Kurtulus et al. (2007) becomes possible and will be performed in a later stage. Further aerodynamic aspects of the test case are given in Wolf et al. (2024).

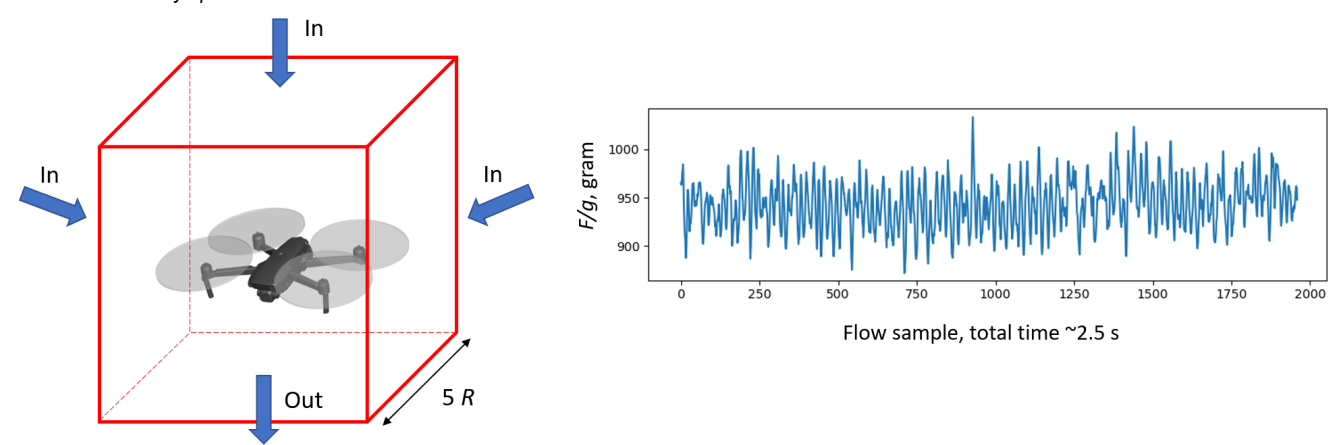


Figure 9 Net total of momentum fluxes, calculated over a cubical control volume containing the quadcopter for a time series of approx. 2.5 seconds. Average vertical force = 943 gram is a good match for the weight of the drone (915 gram), while instantaneous fluctuations up to  $\pm 50$  grams are observed.

## 4. Conclusions and Outlook

The flow around a quadcopter drone has been investigated by Shake-The-Box Lagrangian Particle Tracking of Helium-filled soap bubbles. Due to the large common volume (~ 2m3) and a high number of tracked bubbles, temporally and spatially well-resolved datasets of various flight conditions of the drone could be captured. The application of a scanning approach helped in increasing the effective particle density to over 0.1 ppp. Initial evaluations, which treated the two scanned sub-volumes as independent, already show a high quality of reconstruction. In a later stage, the evaluation will be further developed to allow an integrated reconstruction of multiple (here: two) sub-volumes at a common temporal resolution.

Applying the FlowFit3 data assimilation method yields velocity and pressure fields, that document the complex interaction of the vortex system generated by the four rotors, the development of the common wake and the interaction with the ground, if present. As the whole volume around the drone is captured, a detailed analysis of the forces becomes possible.

Future work will include the development of the integrated Shake-The-Box evaluation, as well as attempting to further increase accuracy and spatial resolution by applying even more advanced interpolation schemes like physics informed neural networks (PINNs, see e.g. Raissi 2019, Zhou et al. 2024).

## References

Bosbach J, Kühn M, Wagner C (2009) Large scale particle image velocimetry with helium filled soap bubbles. *Exp. Fluids* 46:539–47

- CAA UK Civil Aviation Authority (2023) Understanding the Downwash/Outwash Characteristics of eVTOL Aircraft, *Civil Aviation Publication* 2576, https://www.caa.co.uk/CAP2576
- Gesemann S, Huhn F, Schanz D, Schröder A (2016) From noisy particle tracks to velocity, acceleration and pressure fields using B-splines and penalties, *Proceedings of 18th Intern Laser Symp*, Lisbon, Portugal
- Godbersen P, Gesemann S, Schanz D, Schröder A (2024) FlowFit3: Efficient data assimilation of LPT measurements. *Proceedings of 21st Intern Laser Symp*, Lisbon, Portugal
- Hoyer K, Holzner M, Lüthi B, Guala M, Liberzon A, Kinzelbach W (2005). 3D scanning particle tracking velocimetry. *Exp Fluids*, 39, 923-934.
- Jahn T, Schanz D, Schröder A. (2021) Advanced Iterative Particle Reconstruction for Lagrangian Particle Tracking. *Exp Fluids* 62(8), https://doi.org/10.1007/s00348-021-03276-7
- Kozul M, Koothur V, Worth NA et al. (2019) A scanning particle tracking velocimetry technique for high-Reynolds number turbulent flows. *Exp Fluids* 60, 137, https://doi.org/10.1007/s00348-019-2777-3
- Kurtulus, DF, Scarano F, David L (2007) Unsteady aerodynamic forces estimation on a square cylinder by TR-PIV. *Experiments in Fluids*, 42:2, 185-196
- Maas HG, Gruen A, Papantoniou D. (1993) Particle tracking velocimetry in three-dimensional flows part I: Photogrammetric determination of particle coordinates, *Exp Fluids* 15:133–146, https://doi.org/10.1007/BF00190953
- Raissi, M., Perdikaris, P., & Karniadakis, G. E. (2019). Physics-informed neural networks: A deep learning framework for solving forward and inverse problems involving nonlinear partial differential equations. *Journal of Computational Physics*, 378, 686–707.
- Scarano F, Ghaemi S, Caridi GCA, Bosbach J, Dierksheide U, Sciacchitano A (2015) On the use of helium-filled soap bubbles for large-scale tomographic PIV in wind tunnel experiments. *Exp. Fluids* 56:42
- Schanz D, Gesemann S, Schröder A, Wieneke B, Novara M (2013) Non-uniform optical transfer functions in particle imaging: calibration and application to tomographic reconstruction, *Meas Sci Technol* 24:024009
- Schanz D, Gesemann S, Schröder A. (2016) Shake-The-Box: Lagrangian particle tracking at high particle image densities, *Exp. Fluids*, 57:570
- Schanz D et al. (2019) Large-scale volumetric characterization of a turbulent boundary layer flow. 13th international symposium on particle image velocimetry. No. 182. Universität der Bundeswehr München: AtheneForschung

- Schanz, D., Novara, M. & Schröder, A. (2021), Shake-The-Box particle tracking with variable timesteps in flows with high velocity range (VT-STB), 14th International Symposium on Particle Image Velocimetry, Doi:10.18409/ispiv.v1i1.65
- Schröder A, Schanz D (2023) 3D Lagrangian particle tracking in fluid mechanics. *Annual Review of Fluid Mechanics* 55:511-540.
- Schröder D, Leweke T, Stumpf E (2023) High-speed volumetric particle tracking measurements of unstable helical vortex pairs. *Exp Fluids* 64, 141 https://doi.org/10.1007/s00348-023-03679-8
- Wieneke B (2008), Volume self-calibration for 3D particle image velocimetry, *Exp Fluids* 45:549–556
- Wieneke B (2012) Iterative reconstruction of volumetric particle distribution. *Meas Sci Tech*. 24:024008.
- Wei GQ, Ma SD (1991) "Two plane camera calibration: a unified model," 1991 *IEEE Computer Society Conference on Computer Vision and Pattern Recognition*, Maui, HI, USA, 1991, pp. 133-138, doi: 10.1109/CVPR.1991.139675.
- Wolf CC et al. (2019) Experimental study of secondary vortex structures in a rotor wake. *Exp Fluids* 60(11), 175.
- Wolf CC, Schanz D, Schwarz C, Heintz A, Bosbach J, Strübing T, Schröder A (2024) Volumetric Wake Investigation of a Free-Flying Quadcopter using Shake-The-Box Lagrangian Particle Tracking, *Vertical Flight Society 80th Annual Forum*, Montréal, May 7-9, 2024. DOI: 10.4050/F-0080-2024-1161.
- Zhou K, Grauer SJ, Schanz D, Godbersen P, Schröder A, Rockstroh T, Jeon YJ, Wieneke B (2024) Benchmarking Data Assimilation Algorithms for 3D Lagrangian Particle Tracking. *Proceedings* of 21st Intern Laser Symp, Lisbon, Portugal